ACS Sustainable Chemistry & Engineering

pubs.acs.org/journal/ascecg

Research Article

Single-Molecular White Emission of Organic Thianthrene-Based Luminophores Exhibiting Efficient Fluorescence and Room Temperature Phosphorescence Induced by Halogen Atoms

Lesia Volyniuk, Dalius Gudeika, Alexander A. Panchenko, Boris F Minaev, Malek Mahmoudi, Jurate Simokaitiene, Audrius Bucinskas, Dmytro Volyniuk,* and Juozas Vidas Grazulevicius*

Cite This: ACS Sustainable Chem. Eng. 2023, 11, 16914−16925

Read Online

ACCESS | Metrics & More | Article Recommendations | Supporting Information

ABSTRACT: Because of the contradiction of the efficiencies of fluorescence (FL) and room temperature phosphorescence (RTP) under ambient conditions, achievement of the molecular design of efficient monomolecular white emission resulting from the overlapping of FL and RTP is attractive but very challenging. With the aim of obtaining efficient white emission from a single organic molecule, phenyl(thianthren-2-yl)methanone and its tan derivatives with halogen atoms are developed. Single-molecular white emitters are investigated by experimental and theoretical approaches including steady-state and time-resolved spectroscopy, X-ray analyses, and density functional theory calculations. Photoluminescence quantum yields (PLQYs) of white emission of the molecular dispersion of phenyl(thianthren-2-yl)methanone in the rigid host ZEONEX at room temperature are significantly enhanced from 19 to 84% after the removal of oxygen. Based on the results of X-ray analysis of the single crystal, the high PLQY values are partly attributed to the absence of $\pi-\pi$ intermolecular interactions and the low number of weak van der Waals intermolecular stacking due to the strong bending of heterocyclic thianthrene moiety and the high dihedral angle between thianthrene and benzoyl groups. The structural peculiarities of the newly synthesized thianthrene derivatives may result in the development of even more efficient organic monomolecular white emitters.

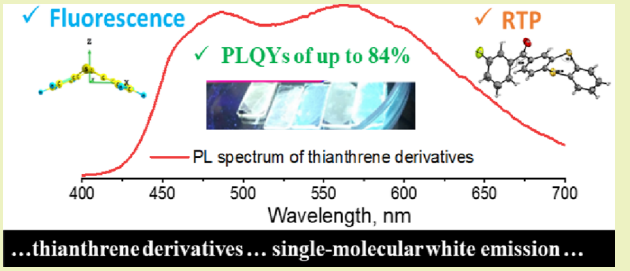

KEYWORDS: *thianthrene, Friedel−Crafts acylation, room temperature phosphorescence, single-molecular white emission, single-crystal X-ray analysis, oxygen quenching*

INTRODUCTION

One of the most relevant energy-saving lighting technologies is solid-state lighting.[1] Inorganic, hybrid, and organic light-emitting diodes (LEDs) are widely known devices of this technology.[2] When such devices are powered by solar cells, the LEDs can directly convert renewable energy to light with higher efficiency in comparison to fluorescent tubes or incandescent light bulbs. In addition, a cleaner environment is reachable with organic LED technology when purely organic functional and light-emitting semiconducting materials with an aromatic backbone are used. White organic LEDs have reached the lighting market[3] due to the possibility to show efficient white emission from multicomponent organic emitters with high white color quality. The main parameters of color quality are Commission International d'Eclairage (CIE1931) chromaticity coordinates (x, y), color temperature (T_C), and color rending index (CRI). White emitters intended for indoor illumination have to be characterized by CIE coordinates close to those of natural light (0.33, 0.33), T_C values in the range from 3000 to 5000 K, and CRI values higher than 80.[4] Even more importantly, these parameters must be stable over the exploitation time of white emitters. However, the color stability of white multicomponent organic emitters can be easily lost because the different components are often characterized by different applicable to all four factors emission lifetimes, different absorption, reabsorption, and emission under different excitation energies. In addition, the shifts of the hole−electron recombination and/or exciton relaxation zones in the device structures under the different external voltages are possible.[5] Single-molecular white emission can potentially allow one to solve problems related to the color instability of white multicomponent organic emitters.[6] Several approaches were proposed for the development of single organic molecules capable of emitting white light. For instance, single-molecular white emission from excimer- or electromer-forming materials

Received: June 30, 2023
Revised: October 24, 2023
Accepted: October 30, 2023
Published: November 20, 2023

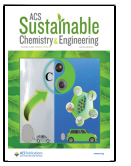

can be observed.[7,8] It can also result from intramolecular energy transfer, intramolecular through-space (exciplex-like) charge transfer, excited-state intramolecular proton transfer, mechanoluminescence, and room temperature phosphorescence (RTP).[9−11] It is supposed that the photoluminescence quantum yields (PLQYs) of single white-light-emitting compounds are commonly low because of the imperfect molecular design and poorly understood mechanism of the white-light emission.[9−11] Indeed, there are a very limited number of RTP-based single-molecular white emitters.[12−17] The single-molecular white emissions were observed either from single crystals or from complicated systems. The PLQY values were typically low. For instance, Tang et.al. developed an RTP-based white emitter with CIE coordinates of (0.33, 0.35) and rather low PLQY of 7.2%.[18] One type of thianthrene crystals showed pure organic single-molecular white emission with PLQY of 47.1%.[16] The copolymers of 4-bromo-1,8-naphthalic anhydride and acrylamide derivatives were developed to emit white light based on RTP, with CIE coordinates of (0.32, 0.33).[19] Their PLQYs were not reported. Organic RTP white-emitting crystal from 2,6-di(carbazol-9-yl)benzonitrile emits delayed white light with a PLQY value of ca. 6%.[19] Phenothiazine boronic ester derivative was recently shown to be an efficient monomolecular white emitter with PLQY of 33%, CIE1931 color coordinates of (0.26, 0.31), color rending index of 73, and color temperature of 8145 K when the rigid polymeric host ZEONEX was used and oxygen was removed.[20] Moreover, efficient RTP compounds typically demonstrate a ratio of phosphorescence quantum yield (Φ_{RTP}) and fluorescence quantum yield (Φ_{FL}) (P2F = Φ_{RTP}/Φ_{FL}) higher than unity in an inert atmosphere. Thus, their RTP should be quenched by oxygen to get white emission. For example, the P2F value of 9.04 was obtained for the most efficient RPT emitter published in ref 13. Thus, the single-molecular white emission of that compound can be expected at P2F of 1 approaching the PLQY value of 9% when RTP is quenched by oxygen. We aimed to achieve highly efficient monomolecular white emission without the need of RTP quenching by oxygen.

In this work, 11 thianthrene derivatives were designed and synthesized, aiming to obtain luminophores with even more efficient single-molecular white emission. Thianthrene moiety and its derivatives may emit strong RTP.[13,21] The thianthrene crystals showed white-greenish photoluminescence with CIE1931 of (0.32, 0.43) in air when RTP is significantly quenched by oxygen.[22] In an inert atmosphere, thianthrene is characterized by weak blue fluorescence and strong green RTP.[21,23] When both efficient fluorescence and RTP are achieved, organic thianthrene-based luminophores with efficient single-molecular white emission can be obtained by appropriate molecular engineering. We aimed to partly prove this prediction in the current study. In this work, phenyl-(thianthren-2-yl)methanone showing RTP-based white emission was synthesized. The white emission was significantly enhanced by the attachment of halogen atoms to the phenyl substituent. Such molecular modifications allow slight changes of the energy mapping of excited singlet (S) and triplet (T) energy levels, leading to the "perfect" energy distribution between S and T states required for efficient white emission, which is caused by the combination of blue fluorescence and orange phosphorescence from a single molecule. The molecular dispersion of (4-fluorophenyl)(thianthren-2-yl)-methanone in ZEONEX demonstrated RTP-based white emission with a high PLQY value of 84% and relatively high quality of white (T_C of ca. 5100 K, CRI of 79, and CIE1931 color coordinates of (0.32, 0.39)).

EXPERIMENTAL SECTION

Instrumentations. Thermogravimetric analysis (TGA) was performed on a TA Instruments TGA Q50 apparatus by recording the weight loss during heating from 0 to 800 °C at the rate of 20 °C/min under a nitrogen atmosphere. Differential scanning calorimetry (DSC) measurements were recorded using a TA Instruments DSC Q2000 equipment under a nitrogen flow of 40 mL/min at heating and cooling rates of 10 °C/min. DSC data are collected in Figure S1.

Cyclic voltammograms (scan rate 100 mV/s) were registered using a micro-Autolab III (Metrohm Autolab) potentiostat−galvanostat. The studied compounds were dissolved in 0.1 M anhydrous dichloromethane with a tetrabutylammonium hexafluoro phosphate electrolyte. The concentration of the solutions was of 10^{-3} M. The measurements were performed in an inert atmosphere using a glassy carbon working electrode, Ag/Ag (0.01 M in anhydrous acetonitrile) reference electrode, and Pt wire counter electrode, whose potential was verified using the ferrocene couple at the end of each set of experiment. CV data are collected in Figure S2.

Edinburgh Instruments FLS980 and Avantes spectrometers were used for the investigation of the photophysical properties of the synthesized compounds. Photoluminescence (PL) spectra were recorded by selecting an excitation wavelength of 330 nm. The after excitation delay time of 1 ms was selected to record phosphorescence spectra at 77 K. A PicoQuant LDH-D-C-375 laser with a wavelength of 374 nm was used as the excitation source for recording the decay curves of fluorescence in the nanosecond range. The decay curves of fluorescence were recorded at the wavelengths of the maximum of the fluorescence spectra. The Edinburgh Photonics μF2 μs lamp with a wavelength of 330 nm was used as the excitation source for recording decay curves of phosphorescence in the microsecond range. The decay curves of phosphorescence were recorded at the wavelengths of the maxima of the spectra of phosphorescence. An FLS980 integrating sphere was used for recording of the PLQY values by an absolute method at room temperature. The PLQY values of the neat films in oxygen-free conditions were obtained by first performing measurements in air using an integrating sphere and then evaluating the increase of PL intensity by placing the films in a vacuum cryostat equipped with a turbo-molecular pump and capable of achieving 10^{-5} Torr pressure. Using the same method, the PL quantum yields of the solutions of the compounds in toluene under ambient and degassed conditions were measured. For the preparation of oxygenated solutions, they were bubbled using a compressed oxygen capsule for 10 min. Deoxygenated solutions were prepared by bubbling argon for 10 min using a quartz cell. The singlet and triplet energies were determined from the onsets of the fluorescence and phosphorescence spectra of the THF solutions recorded at 77 K, respectively. An integral nitrogen reservoir cryostat (Optistat DN2) providing a controlled low-temperature exchange gas environment was used for the characterization of the photophysical properties of the samples from 77 to 300 K in a nitrogen atmosphere. Photophysical data are collected in Figures S3−S6.

We selected the inert polymeric host ZEONEX to study the emission properties of the developed compounds in the solid state. We purchased a ZEONEX 480R from Labochema LT. To deposit the layers of the compounds doped (5%) in ZEONEX, we mixed toluene solutions of ZEONEX and of the tested compounds. ZEONEX was dissolved in toluene to form a solution with a high concentration of 80 mg/mL, whereas the compounds were dissolved in toluene to form solutions with a concentration of 2 mg/mL. The layers were deposited on the precleaned microscope slides with an area of 25 mm^2. The layers were prepared by drop-casting 200 μL of a toluene solution containing ZEONEX and the tested compound. The microscope slides were cleaned before that in an ultrasonic bath with water, acetone, and isopropanol for ca. 10 min each. Afterward,

https://doi.org/10.1021/acssuschemeng.3c04011
ACS Sustainable Chem. Eng. 2023, 11, 16914−16925

Scheme 1. Synthetic Scheme of Compounds T2F, T3F, T4F, T26F, T34F, T2CL6F, T2CL4F, T3CL4F, T23CL, T4Br, and TBO.

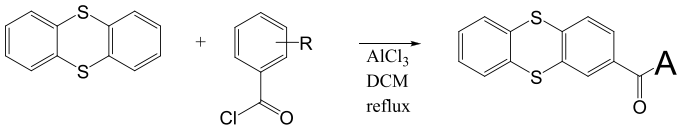

R:	A:					
H			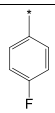		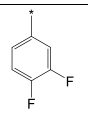	
F	T2F	T3F	T4F	T26F	T34F	TBO
Cl		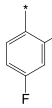	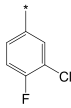		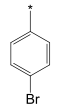	
Br	T2CL6F	T2CL4F	T3CL4F	T23CL	T4Br	

Table 1. Thermal and Redox Characteristics of the Compounds

compound	$T_{d\text{-}5\%}$,°C	T_g, °C	T_{cr}, °C	T_m, °C	$E_{ox1/2vs\ Fc}$, V	$E_{red.1/2vs\ Fc}$, V	[a]IP_{CV}, eV	[b]EA_{CV}, eV
T2F	252	20		88	0.99	−2.09	5.79	2.77
T3F	244	9	71	151	0.97	−2.05	5.77	2.75
T4F	241		98	173	0.96	−2.18	5.76	2.62
T26F	254	20		154	0.99	−2.01	5.79	2.79
T34F	244	17	77	156	0.96	−2.06	5.76	2.74
T2CL6F	265	30		146	0.99	−2.05	5.79	2.75
T2CL4F	274	23		102	0.94	−2.09	5.74	2.71
T3CL4F	253	19	78	177	0.97	−2.06	5.77	2.74
T23CL	287	35		134	1.00	−2.06	5.80	2.74
T4Br	247	28	83	170	0.96	−2.07	5.76	2.73
TBO	256	11	83	142	0.95	−2.17	5.75	2.63

[a]Calculated according to the following equation: $EA_{CV} = e(E_{red.onset} + 4.8)$ [eV]. [b]Calculated according to the following equation: $IP_{CV} = -e(E_{ox.onset} + 4.8)$ [eV].

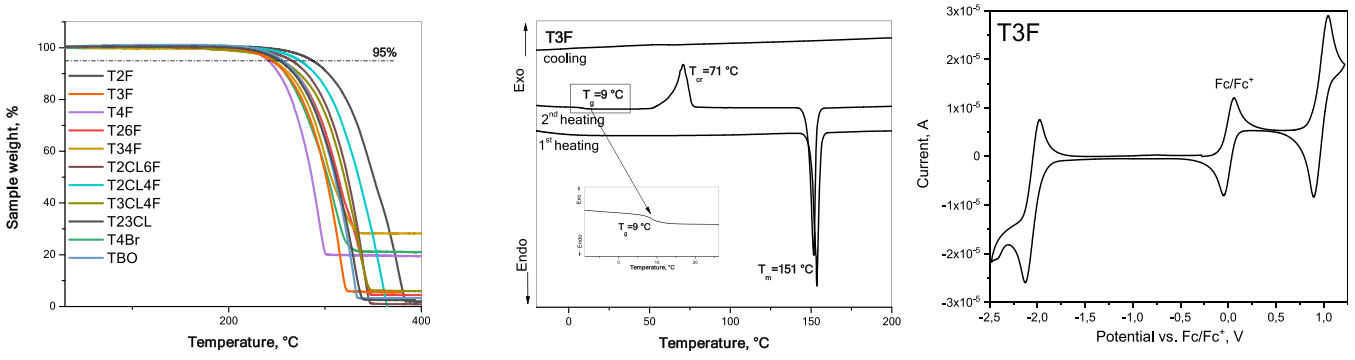

Figure 1. TGA (a) curves of the compounds, DSC (b) curves, and cyclic voltammogram of compound T3F (c).

they were cleaned using the UV Ozone Cleaner from Ossila for 5 min. After the deposition process, the layers were left to dry at 90 °C for ca. 2 h.

RESULTS AND DISCUSSION

Synthesis. Eleven derivatives of thianthrene were obtained by Friedel−Crafts acylation using benzoyl chloride with the different halogen atoms attached to the phenyl ring. The reactions were catalyzed by $AlCl_3$. Good yields of target compounds were achieved by carbon−carbon bond formation, as shown in Scheme 1. All of the target compounds were purified using column chromatography and by recrystallization from the mixtures of chloroform and hexane.

Thermal Properties. Thermogravimetric analysis (TGA) and differential scanning calorimetry (DSC) were used to investigate the thermal and morphological properties of the compounds. The main thermal parameters are summarized in Table 1. All the compounds demonstrated close values of 5% weight-loss temperatures ($T_{d\text{-}5\%}$'s). The $T_{d\text{-}5\%}$ values were in the range of 239−287 °C (Figure 1a). Taking into account that the weights of most of the samples dropped practically to zero in the single stages during the TGA measurements, it can

https://doi.org/10.1021/acssuschemeng.3c04011
ACS Sustainable Chem. Eng. 2023, 11, 16914−16925

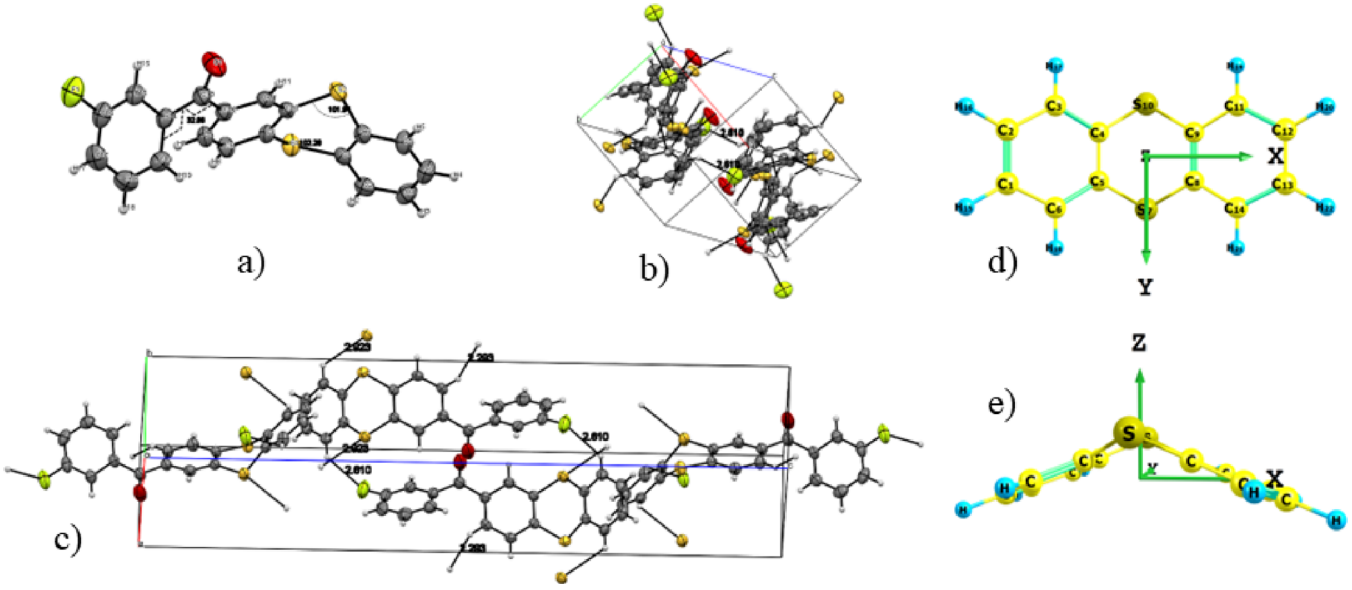

Figure 2. X-ray structure (ORTEP projection) (a) and packing in the crystal structure from different sides (b, c) of compound T3F. An angle at the S···S axis of thianthrene, a torsion angle between thianthrene and acceptor, and intermolecular short distances were measured. The DFT optimized molecular structure of thianthrene molecule in the ground S_0 state: top (d) and side (e) views.

be concluded that $T_{d\text{-}5\%}$'s are the temperatures of the onsets of sublimation of the compounds but not of the thermal degradation. Compounds containing Cl atom(s) (T23CL, T2CL4F, and T2CL6F) showed slightly higher $T_{d\text{-}5\%}$ values than compound TBO due to either slightly higher molecular weights or the different molecular packing in the solid state.

All of the synthesized compounds were obtained after the synthesis and purification as crystalline solids. They showed well-defined melting points (T_m's) in DSC curves (Figure 1b, Figure S1, and Table 1). Glass transitions were observed in the second heating scans at rather low temperatures of 9−49 °C. The lowest T_g of 9 °C was observed for compound T3F apparently because of the small number of sites of intermolecular interactions as evident from X-ray analysis (Figure 2a−c). Low T_g values suggest the usage of rigid hosts (e.g., ZEONEX[24]) for solid-state applications of the compounds. The slow cooling of the melted samples of the compounds (e.g., TBO, T3F, and others) was found to be good condition for crystallization. The crystallization temperatures (T_{cr}'s) were in the range of 71−98 °C (Figure 1b, Table 1). Meanwhile, crystallizations were not observed for compounds T26F, T23CL, and some others (Figure 1b, Table 1).

X-ray Analysis of the Representative Compound and the Theoretically Optimized Structures. Single crystals of one representative compound, T3F, were grown, and single-crystal X-ray analysis was performed. The parameters of its X-ray structure can be deduced using the crystallographic data of T3F deposited in the Cambridge Crystallographic Data Centre with the corresponding CCDC deposition number 2160882. Compound T3F is highly unsymmetrical. This conclusion follows from its Oak Ridge Thermal Ellipsoid Plot (ORTEP) projection (Figure 2a). As is typically expected for the thianthrene fragment based on a 1,4-dithiin structural moiety, the valence <C−S−C angle is of ca. 102°.[25,26] DFT optimization supports the <C−S−C bending valence angle (101.5 and 101.7°). For the dihedral bending angle between two planes of the 1,4-dithiin structural moiety via the S···S axis, our DFT calculation predicts the result $<C_3-C_4-S_{10}-C_9$ = 140.6°. Such dihedral bending of the rigid heterocycle thianthrene can prevent $\pi-\pi$ intermolecular interactions. The DFT optimized structures of the molecules of T3F, T4F, T4Br, and TBO are shown in Figure S7−S10. Twisting between thianthrene and benzoyl groups does not allow the $\pi-\pi$ stacking interactions.[27] The torsion angle of 32.86° between those units is measured by single-crystal X-ray analysis. DFT predicts a dihedral angle C13−C15−C16-C22 = 30.9° (Figure S7)), and this is in a good correspondence to the twisting between the right ring of thianthrene and benzoyl groups. Indeed, $\pi-\pi$ stacking interactions are not observed when analyzing the packing pattern in the single crystal of the molecules of T3F (Figure 2b). The molecules are side-shifted oneswith respect to other in the solid state. In addition, the molecules of T3F in the single-crystal structure are returned with inversion and translational shift one concerning other; i.e., the thianthrene and benzoyl groups of neighboring molecules have short separations (distance of 2.61 Å) through the C−H···F weak van der Waals intermolecular contacts (Figure 2c). These bonds are formed between the fluorine of benzoyl and hydrogen atom of thianthrene of the neighboring molecules.

We have found from DFT calculations that the benzoyl group produces rather strong asymmetry in the thianthrene moiety. The optimized C_4-S_{10} bond length (r = 1.7874 Å) is much longer than the C_9-S_{10} bond (r = 1.7816 Å) (Figure 2d,e). In the lower moiety of the 1,4-dithiin ring, the bonds C_5-S_7 and C_8-S_7 are almost equal (1.786 Å). This is a result of perturbation along the para-position with respect to the C═O group. The similar perturbations of thianthrene symmetry produced by benzoyl moiety are also well seen. The carbon rings in a pure thianthrene molecule that belongs to the C_{2v} point group can really deviate out of the D_{6h} symmetry. However, such deviations from the symmetry are very different in the right and left carbon rings. For example, the bond length $r(C_{11}-C_{12})$ = 1.392 Å is shorter than $r(C_{11}-C_9)$ = 1.399 Å by 0.007 Å, but the difference is higher in the lower part of the carbon ring in the vicinity of the carbonyl group: $r(C_8-C_{14})$ =

https://doi.org/10.1021/acssuschemeng.3c04011
ACS Sustainable Chem. Eng. 2023, 11, 16914−16925

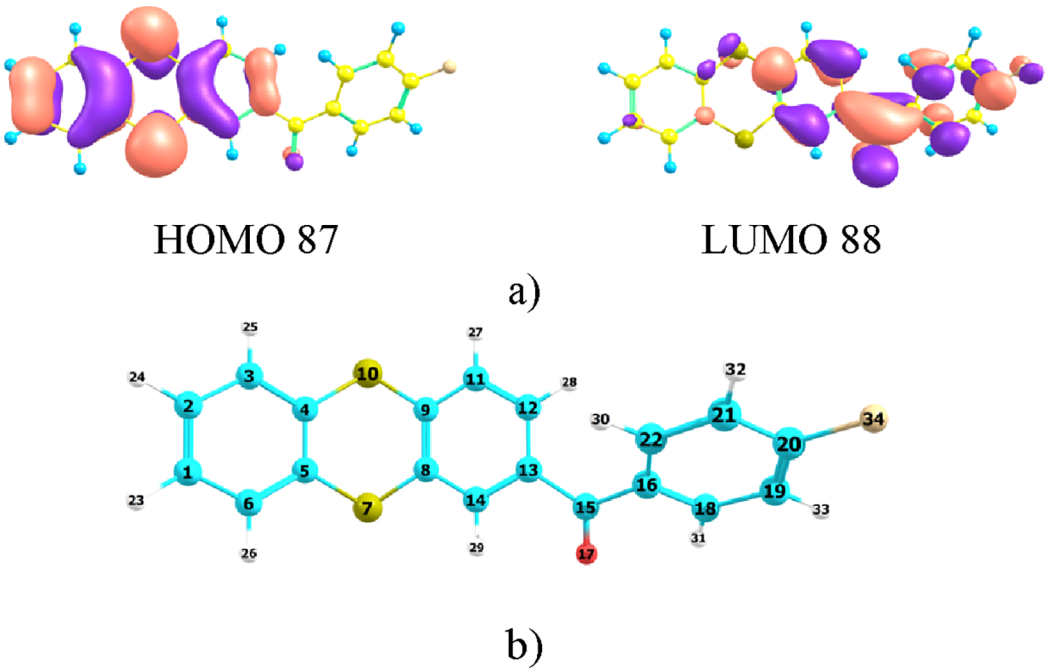

Figure 3. Frontier molecular orbitals (a) and atomic numeration (b) of the optimized structure of T4F in the ground S_0 state.

1.393 Å is much shorter than $r(C_{14}–C_{13})$ = 1.402 Å by 0.009 Å. In the left carbon ring, all such differences are smaller, and all are close to 0.005 Å. The effect of the benzoyl substituent is quite prominent for C−S bonds in all the studied compounds. This distortion leads to essential relaxation of the dipole selection rules in optical absorption and emission spectra, making forbidden transitions in the thianthrene molecule to become allowed for the substituted thianthrenes. This obstacle is very important for the absorption and fluorescence spectra of the synthesized thianthrene derivatives. Of course, the thianthrene core itself has efficient RTP emission because of considerable out-of-plane distortion in the dithiin moiety that provides a large orbital angular momentum change inside the sulfur atoms upon S-T excitation,[28,29] contributing to phosphorescence enhancement according to El-Sayed's rule.[30] The large atomic radius of sulfur supports the twisting distortion, but HOMO−LUMO excitation (Figure 3a) will reduce the twist conformation around the dithiin moiety, inducing the large conformational change upon the S-T transition. This has a big influence on the vibronic SOC effect, S-T mixing, intersysten crossing rate, and RTP yield.[31] But the benzoyl substituents induce additional distortions that strongly reduce the C_{2v} symmetry of the thianthrene core. In combination with benzoyle acceptors, the $n \rightarrow \pi^*$ transition channel of carbonyl group can be added to thianthrene $l \rightarrow \pi^*$ character. All the additional perturbations are the subject of our study.

Redox Properties, Ionization Potentials (IPs), and Electron Affinities (EAs). To investigate the redox properties of the compounds, cyclic voltammetry (CV) measurements were performed recording cyclic voltammograms within the electrochemical window from −2.5 to 1.3 V versus ferrocene. Figure 1c shows the voltammograms of the representative compound T3F. Voltammograms of the other compounds are shown in SI Figure S2. High reduction potentials ($E_{red.1/2}$'s) were obtained for the studied compounds in the very narrow range from −2.18 to −2.01 V. These $E_{red.1/2}$ values are lower than $E_{red.onset}$ of −2.65 V that was reported for thianthrene.[32] These differences are related to the presence of an electron-withdrawing benzoyl moiety. Meanwhile, the presence of halogen atoms practically did not have any strong effects on the reduction properties of the compounds.

The oxidation potentials ($E_{ox.1/2}$'s) also were found in the narrow range from 0.94 to 1.00 V. These oxidation potentials are lower than that of thianthrene (ca. 1.3 V[32]) because of the extended conjugation of the studied compounds. Using the $E_{ox.1/2}$ and $E_{red.1/2}$ data, the corresponding values of the ionization potentials (IP_{CV}'s) and electron affinities (EA_{CV}'s) were obtained (Table 1). The DFT theory allowed the calculation of orbital energies and comparison with the experimental ionization potential and electron affinity data obtained from CV measurements (Table S2). The discussion on the calculated ionization potential and electron affinity data can be found below.

Figure 3a shows the highest occupied molecular orbital (HOMO) of the T4F molecule and its lowest unoccupied molecular orbital (LUMO). The optimized structure of T4F is given in Figure 3b. The former π-orbital of HOMO is almost completely localized at the thianthrene moiety (with a small π-contribution at the oxygen atom of the carbonyl group). This explains the narrow range of oxidation potentials for the whole series of studied compounds. The shift from thianthrene can be explained by additional interelectronic repulsion with the benzoyl group, which makes ionization of the derivatives easier. LUMO represents mostly the antibonding $\pi^*_{C=O}$ orbital conjugated with the nearest aryl groups. That is why the reduction of thianthrene has a completely different nature in comparison to the studied new derivatives. The electron affinity of thianthrene (2.15 eV) is much lower than that of the series of the studied compounds (ca. 2.75 eV in Table 1). Introduction of the benzoyl group into new molecules of the derivatives shifts the center of electron affinity from the thianthrene ring to the bridge between two chromophores, which is held by the carbonyl $\pi^*_{C=O}$ vacancy. Thus, the new

https://doi.org/10.1021/acssuschemeng.3c04011
ACS Sustainable Chem. Eng. 2023, 11, 16914−16925

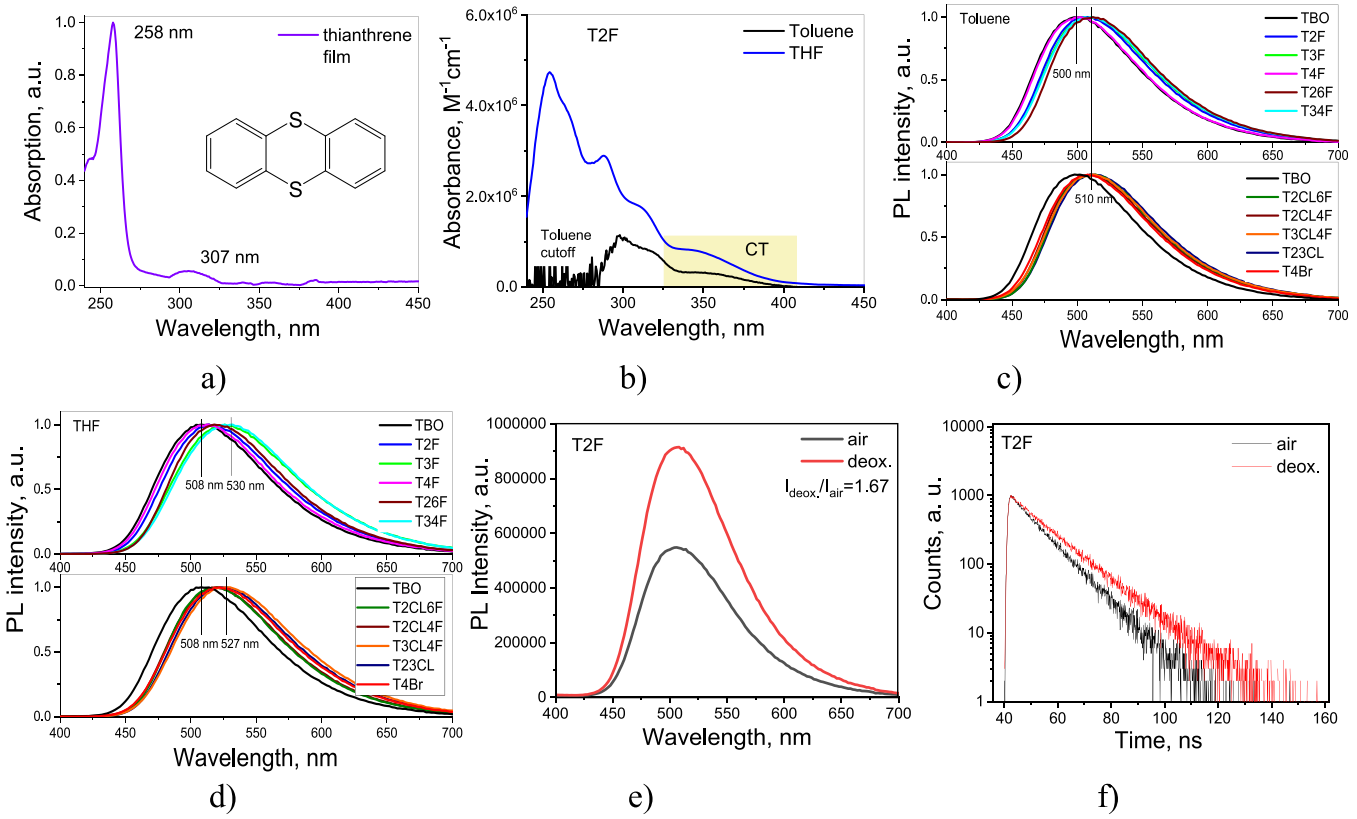

Figure 4. Absorption spectrum (a) of a spin-coated film of thianthrene (the molecular structure of thianthrene is shown in the inset). Absorption spectra (b) of dilute toluene and THF solutions of T2F. PL spectra of dilute toluene (c) and THF (d) solutions of the compounds. PL spectra (e) and PL decay curves (f) of dilute toluene solutions of T2F before (air) and after (deox.) deoxygenation.

incoming electron upon reduction will be distributed between the right thianthrene edge and the benzoyl group (Figure 3a). The properties of HOMO and LUMO wave functions (Figure 3a) correlate well with the redox potentials of the compounds and explain their electronic spectra. The structures of the frontier orbitals pretty well satisfy the general requirements, which have to be fulfilled to get efficient RTP, PL, and spin−orbit coupling (SOC) induced by the mixing of the S and T excited states.[33] To achieve this goal, one needs proper energy alignment of the S-T states with various orbital characters with local *n, l, π* symmetry and the *σ*−*π* mixing induced by the noncoplanarity of the D−A system.[34] The SOC matrix element between S_3 and T_1 states is responsible for the RTP transition dipole moment in thianthrene according to the perturbation-theory scheme where phosphorescence intensity is borrowed from the allowed S_3−S_0 transition. This is often achieved in the donor−acceptor (D−A) compounds with noncollinear and even near-perpendicular D−A planes.[35] At such D−A geometries, the well-separated frontier MOs are usually obtained.[30] Such molecular orbitals (shown in Figure 3a) illustrate the typical intramolecular charge transfer (CT) character for the HOMO−LUMO excited state. HOMO shows the inclined 3p AO on the upper sulfur atom (Figure 3a) that strongly deviates from the common *π*-orientation. Such type of 3p AO is known as *l* orbital according to the Kasha classification (the best example is the N atom orbital in the nonplanar aniline molecule).[36] Accounting for *l* orbital leads to the single-center SOC integral contribution in spin−orbit coupling calculation between $^3l\pi^*$ and $^1\pi\pi^*$ states.[33,36]

The DFT calculated energies of the frontier orbitals are compared to the experimental data in Table S1. In spite of the typical shift of ca. 0.5 eV usually obtained for the B3LYP functional between frontier MO energy and redox parameters produced by CV measurements, the theoretical data reasonably correlate with the results of CV experiment This illustrates the energy gap between redox parameters, where the theory−experiment deviation is quite small (Table S1).

Theoretical Study and Photophysical Properties of the Compounds. It is relevant to consider our theoretical interpretation of the thianthrene spectral properties (Figure 4a) before analysis of the experimental absorption and emission spectra of the synthesized compounds (Figure 4b−d). Thianthrene itself provides efficient RTP, but its absorption at wavelengths exceeding 280 nm is rather weak, which limits the possible application of thianthrene as an optical ratiometric sensor. The molecule is nonplanar with similar but symmetrical distortions in 1,4 dithiin moiety like those observed in thianthrene derivatives (Figure 2d,e); the S_0 ground state of thianthrene belongs to the C_{2v} symmetry point group, and the excited states calculations were performed at this optimized geometry.

Geometry optimization of the excited T_1 and S_1 states shows some asymmetrical distortions; at the same time, the optimized T_1 state is closer to the coplanar structure. Because of the absence of the C_{2v} symmetry, spin-vibronic calculations for phosphorescence analysis are impossible with our facilities. Thus, we used the S_0 ground-state structure for the qualitative discussion of SOC effects on RTP.

Our TD DFT calculations (Figure S11 and Table S2) explain the absence of intense absorption at the wavelengths above 280 nm by thianthrene. The intense band at 258 nm is predicted as the EDTM-allowed $X^1A_1 \rightarrow 2^1B_1$ transition with

https://doi.org/10.1021/acssuschemeng.3c04011
ACS Sustainable Chem. Eng. 2023, 11, 16914−16925

the large oscillator strength (f = 0.29) and polarization on the long axis (x). The lowest singlet excited state 1^1A_2 produces a weak band at 307 nm. The corresponding $X^1A_1 \rightarrow 1^1A_2$ transition is EDTM-forbidden but is allowed in the framework of the magnetic selection rule. In spite of the large magnetic dipole transition moment (1.58 μ_B), the oscillator strength for this band is rather low ($f = 0.89 \times 10^{-5}$), and a large part of the observed band intensity is explained by the vibronic perturbation and intensity borrowing from the allowed $X^1A_1 \rightarrow 2^1B_1$ transition.

The quadratic response DFT calculation explains the very weak absorption in the near-UV region (380 and 360 nm) by S-T transitions with low oscillator strengths of about 10^{-7}−10^{-8} and a radiative lifetime for thianthrene phosphorescence of 48 ms. Strong SOC perturbations in thianthrene are determined by the nonplanar structure and σ−π mixing at sulfur atoms that lead to the single-center SOC integral contributions to the S-T matrix elements. Very similar SOC effects are expected in the synthesized thianthrene derivatives because the nonplanar distortion in the 1,4-dithiin moiety is almost the same.

For the investigation of electronic structures of the studied compounds in the ground state, the absorption spectra of dilute toluene and tetrahydrofuran (THF) solutions were recorded. They are plotted in Figure 4b and Figure S3a. Low-energy bands in the range from ca. 320 to 390 nm were observed in the spectra of the solutions of all of the compounds. This band is red-shifted in comparison to locally excited (LE) transitions of thianthrene that peaked at 258 and 307 nm (Figure 4a). The low-energy band is assigned to intramolecular CT transitions from thianthrene moiety to the antibonding $\pi^*_{C=O}$ orbital and phenyl ring nonbonding MO having different accepting abilities due to the presence of halogen atoms.

TD DFT calculations fully support this suggestion (Figures S12−S14, Tables S3−S8). The first absorption band represents mostly the HOMO−LUMO single-electron excitation (Figure 3a, Table 2) and almost pure charge transfer transition. For the solutions in polar THF, these CT bands are enhanced (Figure 4b, Figure S3a) because of additional polarization from the polar environment, which leads to more delocalized π-electron densities among two noncoplanar D−A planes. The electric dipole transition moment (EDTM) for the CT band depends on common HOMO−LUMO contributions from those atoms that are far separated from each other. This means that the small contributions from the left side of LUMO and a small coefficient at the oxygen atom in the HOMO expansion are important for the CT band intensity, which is determined by the square of the EDTM value. That is why the polarizing effect of THF solvent on the CT band intensity is so prominent because of the EDTM enhancement (Figure 4b, Figure S3a).

Table 2. Comparison of the Structural Parameters of the Molecule of T4F Optimized by the TD-DFT Method in the Ground and Excited States

bond length	S_0 state	S_1 state	bond length	S_0 state	S_1 state
C_1−C_2	1.396	1.414	C_9−S_{10}	1.782	1.769
C_3−C_4	1.400	1.416	C_4−S_{10}	1.787	1.734
C_4−C_5	1.403	1.430	C_{15}−O_{17}	1.226	1.260
C_5−C_6	1.400	1.418	C_{15}−C_{16}	1.498	1.478
C_5−S_7	1.786	1.734	C_{20}-F_{34}	1.346	1.355
C_8−S_7	1.786	1.757	C_{16}−C_{18}	1.405	1.415

The second excited singlet state S_2 at ca. 350 nm is attributed to HOMO-2 → LUMO excitation that corresponds mostly to the locally excited benzoyl moiety with an essential nπ^* character at the C═O group and a small CT contribution. TD DFT calculations predict very low intensity for this $S_0 \rightarrow S_2$ transition in the cases of all studied molecules, but it can borrow intensity from the near-lying stronger transitions via vibronic perturbations.

The next more intense band $S_0 \rightarrow S_3$ (f = 0.11) at 314 nm (observed for T4F, T2F, T3F, etc.) represents CT_2 transition or HOMO-1 → LUMO excitation (Figures S12−S14, Tables S3−S8). This second D−A charge-transfer band (from the left part of thianthrene to benzoyl) includes $\pi\pi^*$ excitation of benzoyl and $\pi\pi^*$ in the right part of the thianthrene moiety. The particularly large charge-transfer to the π^* orbital of the C═O group can be mentioned (Figures S12−S14). The band observed at 314 nm band is shifted and deformed in the cases of some molecules (TBO, T2Cl4F), especially for the solutions in polar THF (Figure 4b, Figure S3a).

The close-lying S_4 state provides absorption at 294 nm of similar intensity (f = 0.096 in T4F). This is the HOMO → LUMO+1 excitation that corresponds to the π−π^* transition inside the thianthrene moiety with simultaneous CT to benzoyl (Figures S12−S14). For the thianthrene molecule itself, this is the S_2 state ($^1A_1$, Table S2). The corresponding thianthrene band is blue-shifted to 277 nm and forms a wing of the intense band at 258 nm. The intensity of the $S_0 \rightarrow S_4$ absorption depends on the halogen positions according to our TDDFT calculations. The oscillator strength of the solution of T3F in the polar solvent (f = 0.067) is much lower than that of the corresponding solution of T2F (f = 0.117).

Solvents can increase the CT band intensity. Geometry optimization of the first excited singlet S_1 state performed by TD DFT does not reveal the change of its CT nature and leads to an increase of the C−C bond lengths in the left benzene ring of the thianthrene moiety. The excited electron leaves the HOMO, which is a bonding orbital with respect to C1−C2, C3−C4, C4−C5, and C5−C6 bonds. Thus, their bonding character is decreased upon HOMO−LUMO excitation. All these chemical bonds of the left benzene ring are getting weaker and longer by ca. 0.02 A upon S_0−S_1 transition (Figure 4, Tables S3−S8). The opposite distortions occur in the C−S bonds upon excitation because HOMO is an antibonding orbital with respect to those bonds (Figure 3). Thus, they get stronger when an electron experiences the HOMO−LUMO jump (Figure 3, Tables S3−S8) because those positions are not active in the LUMO. The electron that leaves HOMO does not provide an antibonding character for the C−S bonds anymore, and they are shortened upon excitation. When the excited electron occupies the LUMO level upon $S_0 \rightarrow S_1$ transition, the C═O bond becomes weaker because of the strong antibonding character of the LUMO. At the same time, the C15−C16 link of the carbonyl group is shortened by 0.02 Å because the LUMO increases its bonding character (Figure 3, Tables S3−S8). The LUMO is a nonbonding orbital for the fluorobenzene ring. Thus, there are no big distortions upon $S_0 \rightarrow S_1$ transition in that ring besides small prolongations of the C16−C bonds, which are obvious from their weak antibonding features (Figure 3, Tables S3−S8). The LUMO is also slightly antibonding for the C−F bond that is prolonged by 0.01 Å upon CT transition (Tables S3−S8). The change of the

https://doi.org/10.1021/acssuschemeng.3c04011
ACS Sustainable Chem. Eng. 2023, 11, 16914−16925

Table 3. Photophysical Parameters of the Studied Compounds

compound	I_{deox}/I_{air}	τ_{Fl}, ns [d]toluene	PLQY, %	S_1, eV	T_1, eV [e]MeTHF	ΔE_{ST}, eV	[a]$PLQY_{Fl}$, %	[b]$PLQY_{Phos.}$, % [f]ZEONEX	[c]$PLQY_{vac}$, %	$\tau_{Phos.}$, ms
T2F	1.67	13.59	47	2.90	2.56	0.34	10	5	15	12.69
T3F	1.37	13.22	38	2.93	2.60	0.33	16	7	23	11.90
T4F	1.42	13.60	44	2.96	2.58	0.38	42	42	84	13.67
T26F	1.58	15.22	53	2.83	2.48	0.35	32	11	43	10.00
T34F	1.47	13.28	57	2.94	2.58	0.36	16	7	23	12.91
T2CL6F	1.17	15.37	35	2.86	2.48	0.38	27	11	38	13.88
T2CL4F	1.27	15.05	40	2.88	2.54	0.34	24	10	34	13.20
T3CL4F	1.22	13.35	35	2.95	2.58	0.37	15	7	22	12.58
T2CL	1.33	14.82	40	2.9	2.54	0.36	31	14	45	11.92
T4Br	1.4	12.85	39	2.95	2.61	0.34	14	7	23	12.27
TBO	1.34	12.77	35	2.95	2.59	0.36	10	9	19	12.75

[a]Absolute PLQY values of fluorescence measured using an integrating sphere in air. [b]Calculated PLQY values of RTP ($PLQY_{Phos}$ at vacuum) by the formula $PLQY_{Phos.} = PLQY_{vac} - PLQY_{Fl}$. [c]Calculated total PLQY values ($PLQY_{vac}$) by the formula $Area_{vac}/Area_{air} = PLQY_{vac}/PLQY_{air}$, where $Area_{vac}$ and $Area_{air}$ are integrated areas of PL spectra recorded in vacuum and air, respectively (Figure 5b, Figure S3). [d]Deoxygenated toluene solutions. [e]Taken from onsets of PL and phosphorescence (Phos.) spectra at 77K. [f]Films of the compounds (5 wt %) doped in ZEONEX at room temperature and in a vacuum.

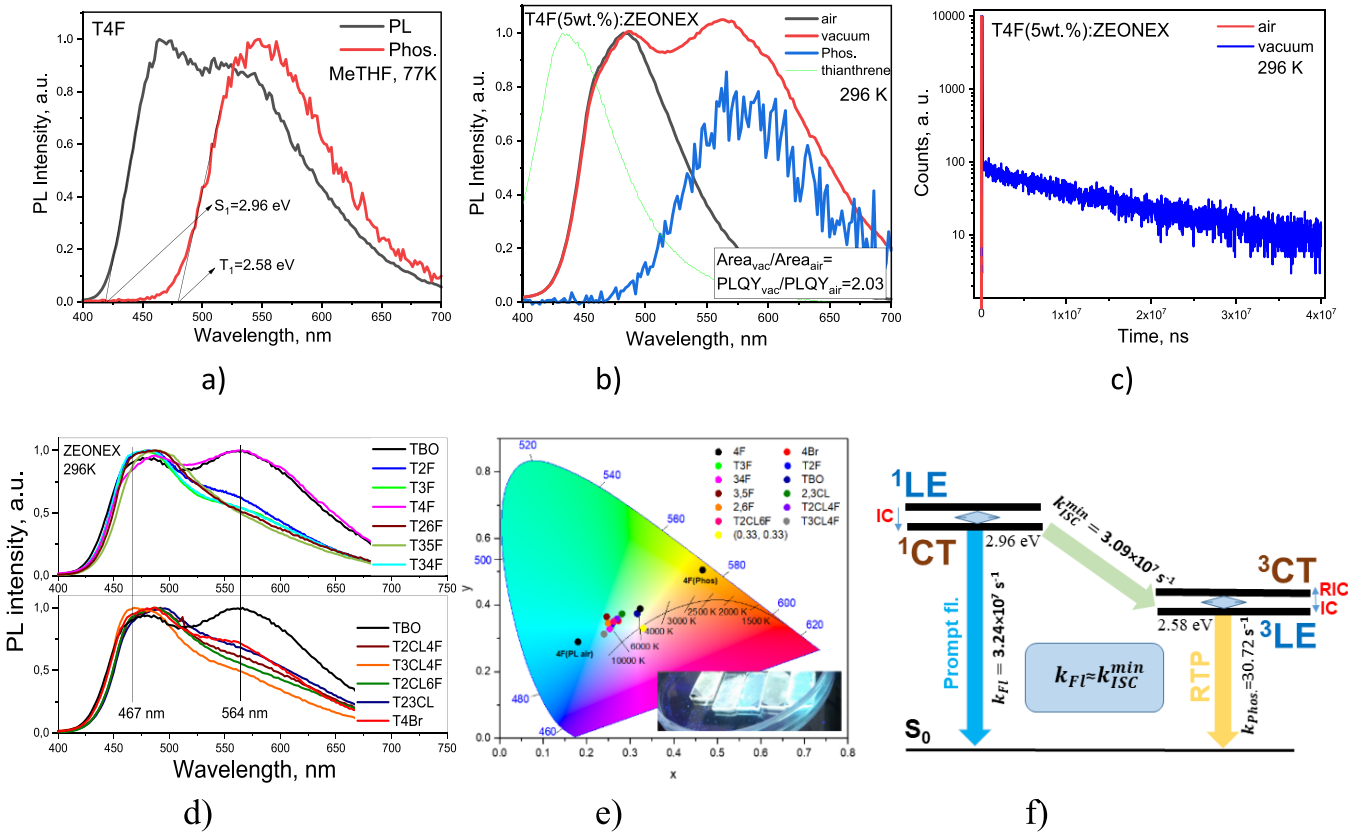

Figure 5. PL and Phos spectra of MeTHF solutions at 77K (a); PL and Phos spectra (b); and the Phos. decay curve (c) of the sample of 4F (5 wt %) doped in ZEONEX recorded at 296 K and in a vacuum; PL spectra (d); $PLQY_{Fl}$, $PLQY_{Phos.}$, and CIE1931 color coordinates (e) of the film of the compound (5 wt %) doped in ZEONEX recorded at 296 K and in a vacuum. Inset: photos of the molecular dispersions of TBO, T4F, T3CL4F, T4Br, and T3CL6F (from left to right, respectively) in ZEONEX in an inert atmosphere under UV excitation. Schematic energy diagram (f) representing relaxation processes of compound 4F. IC and RIC are internal conversion (IC) and reverse IC (RIC), respectively.

position of the halogen substituent in the T3F molecule provides a small but essential change in the LUMO structure (Figure S12, LUMO of T3F). The fluorine position is inactive for LUMO as well as the C1 atom position in contrast to the situation with the T4F isomer (Figure 3b). Thus, the intensity of the CT band of the solution of isomer T3F in polar THF is lower. Thus, the polarization effects increase the shown trend.

THF solutions of thianthrene derivatives exhibited red-shifted PL spectra in comparison to the corresponding PL spectra of toluene solutions because THF is more polar than toluene (Figure 4c,d). The different combinations of halogen atoms attached to the phenyl ring cause slightly different positions of their PL spectra. The peaks in the ranges 500−510 and 508−530 nm were observed for toluene and THF

https://doi.org/10.1021/acssuschemeng.3c04011
ACS Sustainable Chem. Eng. 2023, 11, 16914−16925

solutions, respectively. This shift is well reproduced in our quantum chemical TDDFT calculations (Table 4). Emissions of the compounds in solutions should be related to prompt fluorescence (PF), the lifetimes of which were found in the nanosecond range (Table 3). The calculated $S_0 \leftarrow S_1$ transition dipole moment for PF provides a radiative lifetime of ca. 23 ns for T4F. This value is in qualitative agreement with the results of the experimental measurements. The observed PF lifetime is 13.6 ns (Table 3). Apparently, emission quenching additionally diminishes the observed τ value.

The thianthrene core may act as RTP-promoting chromophore species, able to provide efficient intersystem crossing (ISC), because of strong SOC induced by the sulfur atoms in nonplanar 1,4-dithiin moiety. The phosphorescent properties of its derivatives can be tuned by substituents.[36] Accounting for $l\pi^*$, $n\pi^*$, and $\pi\pi^*$ states can be used to explain the phosphorescent properties, high ISC rate, and triplet formation yield in benzoyl derivative of thianthrene. Accounting for $l\pi^*$, $n\pi^*$, and $\pi\pi^*$ states can be used to explain the phosphorescent properties, high ISC rate, and a triplet formation yield of benzoyl derivative of thianthrene. The *l*-orbital has a large localization at the sulfur atom as 3p AO whose axis is declined with respect to the symmetry plane of the relevant π-MO; *n*-orbital is actually the corresponding σ-MO with strong localization at the sulfur and oxygen atoms. Because the SOC operator includes the orbital angular momentum part, which produces rotation of all AO wave functions around axes, this anisotropy of all mentioned orbitals leads to large one-center SOC contributions from relatively heavy S and O atoms. Thus, the SOC matrix elements between S and T states of those $l\pi^*$, $n\pi^*$, and $\pi\pi^*$ configurations provide an increase of ISC and RTP rates.

White Emission and Oxygen Quenching. It should be noted that the PF intensity and PF lifetimes of the compounds are very sensitive to the presence of oxygen in the solutions (Figure 4e,f, Figure S3). For example, the deoxygenated toluene solution of T2F showed more intense PF by a factor of 1.67 than in case the air equilibrated solution (Table 3). The enhancement of the signals was also observed by recording the corresponding PF decay curves (Figure 5c). Similar behaviors were detected for the solutions of the other compounds studied (Figure S3, Table 3). Fluorescence intensity enhancement is apparently not related to the reverse intersystem crossing of energy from triplet excited states to singlet excited states. Delayed fluorescence was not observed for deoxygenated toluene solutions of the compounds. The compounds are characterized by the relatively high triplet−singlet energy splittings (ΔE_{ST} higher than 0.3 eV (Figure 5a, Figure S4, and Table 3)).[37] On the other hand, nonradiative losses of excited CT states of the compounds decreased after oxygen removal from the solutions. The nonradiative losses of fluorescence are apparently related to the ISC relaxation from singlet to triplet excited states. When the organic chromophore is in collision with the triplet oxygen molecule, the T-S transitions inside the chromophore moiety are not forbidden by the spin selection rule for the whole collision complex.[38] Thus, the high concentration of oxygen in the solvent leads to the quenching of both the fluorescence and phosphorescence of the organic chromophore. The RTP quenching is more efficient than that of PL due to the spin-allowed T-T energy transfer to oxygen with the singlet oxygen generation.[38] The quantum chemical calculations show that the presence of oxygen in organic solvent diminishes the radiative rate constant for the radiative transition $S_1 \rightarrow S_0$ (fluorescence) because its dipole transition moment is depleted by intensity borrowing for various forbidden bands.[38,39] In contrast, the absence of oxygen leads to the less efficient ISC and the higher radiative rate of the excited singlet state manifested as the enhanced PF intensity. As a result, the deoxygenated toluene solutions showed PLQYs in the range from 35 to 57% and PF lifetimes of 12.77−15.37 ns. Considering compound TBO as the reference, the increased PLQY and PF lifetimes of other compounds containing halogen atoms were obtained (Table 3).

These PLQY values are still much lower than 100% apparently because of the incomplete restriction of ISC by deoxygenation because the intrinsic SOC inside the organic chromophore still remains. Organic compounds with efficient ISC typically show RTP.[37,40] The emission spectrum of the T4F molecule calculated by the TDDFT method at the optimized geometry in the S_1 excited state is given in Table 4. It is similar to those of other halogen derivatives. The lowest triplet state, T_1, produces phosphorescence at 605 nm.

Table 4. Emission Spectrum of the T4F Molecule at the Optimized Geometry in the S_1 Excited State

state	λ, nm	oscillator strength *f*	wave function	ΔE, eV
T_1	605	0	0.65(87−88)−0.20(87−89)	2.05
S_1	497	0.058	0.70(87−88)	2.50
T_2	451	0	0.58(85−88)	2.75
T_3	428	0	0.59(87−89)	2.90
S_3	357	0.009	0.65(87−89)	3.47

Vibrational effects of organic molecules typically hinder emissive relaxation of long-living triplets at room temperature.[41] Therefore, such effects should be taken into account when studying RTP properties of organic materials. Usage of rigid hosts (such as inert polymer ZEONEX,[24] polystyrene,[42] or poly(methyl methacrylate)[43]) is one of the good approaches that allows efficient prevention of vibrational quenching effects of the triplet organic molecules.[35] The RTP properties of the layers of the compounds (5 wt %) doped in ZEONEX were studied (Figure 5b−f, Figure S4). In air, because of the low polarity of ZEONEX,[24] the films of the molecular dispersions of the compounds in the ZEONEX showed slightly blue-shifted PL spectra in comparison to corresponding spectra of the polar solutions (Figures 4c,d and 5, Figure S4). That fluorescence is CT in nature. The spectra are observed in a different spectral range than the LE fluorescence of thianthrene in solid state (Figure 5b).

After O_2 evacuation, an additional low-energy band (shoulder) appeared. This band is attributed to RTP because of its similarity to the phosphorescence spectra of the corresponding frozen THF solutions recorded at 77K (Figure S4). Emissive relaxation of the triplet states of the compounds leads to an increase in the corresponding PLQY values. For example, the layer of TBO is characterized by PLQYs of 10 and 19% in air and in vacuum, respectively (Table 3). The calculations of PLQYs of the films under a vacuum were carried out according to the procedure described elsewhere (see also footnotes of Table 3).[13] The total PLQY values of practically all other compounds were higher than those of TBO. Figure 5 and Figure S4 show RTP spectra that were separated from fluorescence spectra using a delay time after excitation of 1 ms. The compounds were found to have RTP

https://doi.org/10.1021/acssuschemeng.3c04011
ACS Sustainable Chem. Eng. 2023, 11, 16914−16925

Table 5. Relaxation Rates and Color Parameters of the Thianthrene Derivatives

compound	k_{Fl}, $\times 10^7$ s^{-1}	k_{ISC}^{max}, $\times 10^7$ s^{-1}	$k_{Phos.}$, s^{-1}	k_{ISC}^{min}, $\times 10^7$ s^{-1}	CIE (x, y)	CRI	T_C, K
T2F	3.46	3.90	3.94	0.37	(0.26, 0.34)	71	7879
T3F	2.87	4.69	5.88	0.53	(0.26, 0.33)	73	8123
T4F	3.24	4.12	30.72	3.09	(0.32, 0.39)	79	5101
T26F	3.48	3.09	11.00	0.72	(0.25, 0.35)	70	8279
T34F	4.29	3.24	5.42	0.53	(0.25, 0.33)	74	8493
T2CL6F	2.28	4.23	7.93	0.72	(0.26, 0.35)	74	7559
T2CL4F	2.66	3.99	7.58	0.66	(0.27, 0.36)	74	7081
T3CL4F	2.62	4.87	5.56	0.52	(0.24, 0.31)	72	9753
T23CL	2.70	4.05	11.74	0.94	(0.28, 0.37)	74	6549
T4Br	3.04	4.75	5.70	0.54	(0.27, 0.35)	73	7011
TBO	2.74	5.09	7.06	0.70	(0.32, 0.37)	79	5275

lifetimes ranging from 10.00 to 13.88 ms (Figure 5c, Figure S5, Table 3). The intensities of PF and RTP bands are comparable in the case of TBO and T4F, resulting in CIE1931 color coordinates of (0.32, 0.37) and (0.32, 0.39), respectively, which are close to (0.33, 0.33) of natural white (Figure 5e, Table 5). In addition, relatively high CRI values of 79 were obtained for TBO and T4F (Table 5). Optimization of the concentration of compounds in ZEONEX can allow additional optimization of the CIE1931 color coordinates according to the user needs (Figure S6, Table S9).

For understanding of the mechanism of the white-light emission of the studied compounds in more detail, the rate constants of radiative (fluorescence) (k_{Fl}) and nonradiative (k_{nr}) deactivation of singlets, the rate constants of radiative (RTP) deactivation of triplets ($k_{Phos.}$), and the maximum (k_{ISC}^{max}) and minimum (k_{ISC}^{min}) rate constants of ISC were calculated using the following formulas (Table 5):

$$k_{Fl} = \frac{\eta_{Fl}}{\tau_{Fl}} \quad (1)$$

$$k_{nr} = \frac{1 - \eta_{Fl}}{\tau_{Fl}} \quad (2)$$

$$k_{Phos.} = \frac{\eta_{Phos.}}{\tau_{Phos.}} \quad (3)$$

$$k_{ISC}^{min} = \frac{\eta_{Phos.}}{\tau_{Fl}} \le k_{ISC} \le \frac{1 - \eta_{Fl}}{\tau_{Fl}} = k_{ISC}^{max} \quad (4)$$

In these formulas, the maximum rate constant of ISC was obtained assuming that nonradiative deactivation of all singlets is related to the ISC processes ($k_{ISC}^{max} = k_{nr}$).[30] The highest $k_{Phos.}$ value of 30.72 s^{-1} was obtained for compound T4F with the highest PLQY value of 84% (Tables 3 and 5). Reflecting the most efficient RTP, the highest k_{ISC}^{min} value of $3.09 \times 10^7 s^{-1}$ was also observed for compound T4F. This k_{ISC}^{min} value is practically the same as its k_{Fl} value ($3.24 \times 10^7 s^{-1}$). Such observation allows us to suggest that the balance between the rate constants k_{Fl} and k_{ISC} is required for the activation of efficient fluorescence and RTP after reaching the "perfect" energy distribution between singlet and triplet states (Figure 5f). The special energy mapping of excited singlet and triplet energy levels is required for the perfect energy distribution.

Halogen substituents attached to benzoyl moiety do not influence the RTP and the rate constant $k_{Phos.}$ as internal heavy atom (IHA) effect rather peculiar; for example, the halogen orbital admixtures of T4F and T3F in the low-lying T and S states (Figures S15–S16, Tables S3–S8). The SOC mixing between S and T states in T4F is more efficient being mainly arranged by nonplanarity of the thianthrene moiety and sulphur atoms contributions, but simultaneously SOC is sensitive to the halogen IHA effect.

CONCLUSIONS

Eleven thianthrene-based luminophores containing different halogen atoms were synthesized. All the compounds show bright fluorescence in solutions and in the solid state with PLQYs reaching 57 and 42%, respectively. The compounds doped in rigid polymeric host at room temperature also exhibit efficient phosphorescence with PLQYs reaching 42%. Because of the equally efficient blue fluorescence and orange room temperature phosphorescence, one compound demonstrates white emission with high PLQY value of 84% and relatively good quality of white (T_C of ca. 5100 K, CRI of 79, and CIE1931 color coordinates of (0.32, 0.39)). The key reason for such white emission of single molecules is the balance between the rates of radiative transition from singlet states (3.24×10^7 s^{-1}) and intersystem crossing (3.09×10^7 s^{-1}). Such photophysical properties of the synthesized thianthrene derivatives can be explained by their structural peculiarities. The C–S bonds in the upper part of the thianthrene ring are different. The C_9–S_{10} bond is shorter by 0.0052 Å than the C_4–S_{10} bond. This is a pure result of perturbation by the carbonyl group. It is shown that the effect of halogen atoms on the asymmetry of the thianthrene ring is rather small. The main effect on the para-asymmetry of thianthrene with respect to C═O substituents is caused by this carbonyl group. The C_9–S_{10} link is situated along the para-diagonal C_9–C_{13}–C_{15}, and the strongly polar carbonyl group (acceptor) provides a strong influence on the bond length.

The strong twist around the S···S axis being pertinent to thianthrene provides efficient σ–π mixing of orbitals, which is responsible for large SOC contributions at sulfur atoms to the ISC perturbations between S and T states. At the same time, the carbonyl group represents an efficient link for hyperconjugation between noncoplanar π-systems of the D–A moieties. The corresponding dihedral angle between D–A π-systems is far from orthogonality (ca. 34°), and the right terminal part of thianthrene is well conjugated with the π-system of benzoyl moiety. Thus, several new absorption bands starting from the near-UV region occur in the synthesized D–A compounds of the mixed complicated CT nature, including also local π–π^* excitations in the right ring of thianthrene and in benzoyl.

https://doi.org/10.1021/acssuschemeng.3c04011
ACS Sustainable Chem. Eng. 2023, 11, 16914–16925

■ ASSOCIATED CONTENT

Supporting Information

The Supporting Information is available free of charge at https://pubs.acs.org/doi/10.1021/acssuschemeng.3c04011.

Detailed descriptions of the synthesis and identification, DSC curves, cyclic voltammograms, photophysical data, and additional descriptions of theoretical investigations of the compounds (PDF).

Crystallographic information file of compounds used in the study (CIF)

■ AUTHOR INFORMATION

Corresponding Authors

Dmytro Volyniuk − *Department of Polymer Chemistry and Technology, Kaunas University of Technology, Kaunas LT-51423, Lithuania;* orcid.org/0000-0003-3526-2679; Email: dmytro.volyniuk@ktu.lt

Juozas Vidas Grazulevicius − *Department of Polymer Chemistry and Technology, Kaunas University of Technology, Kaunas LT-51423, Lithuania;* orcid.org/0000-0002-4408-9727; Phone: +37037300193; Email: juozas.grazulevicius@ktu.lt; Fax: +37037300152

Authors

Lesia Volyniuk − *Department of Polymer Chemistry and Technology, Kaunas University of Technology, Kaunas LT-51423, Lithuania*

Dalius Gudeika − *Department of Polymer Chemistry and Technology, Kaunas University of Technology, Kaunas LT-51423, Lithuania*

Alexander A. Panchenko − *Department of Chemistry and Nanomaterials Science, Bohdan Khmelnytsky National University, Cherkasy 18031, Ukraine;* orcid.org/0000-0001-7669-1424

Boris F Minaev − *Department of Chemistry and Nanomaterials Science, Bohdan Khmelnytsky National University, Cherkasy 18031, Ukraine; Department of Physics and Astronomy, Uppsala University, Uppsala SE-75121, Sweden;* orcid.org/0000-0002-9165-9649

Malek Mahmoudi − *Department of Polymer Chemistry and Technology, Kaunas University of Technology, Kaunas LT-51423, Lithuania;* orcid.org/0000-0002-9580-6220

Jurate Simokaitiene − *Department of Polymer Chemistry and Technology, Kaunas University of Technology, Kaunas LT-51423, Lithuania*

Audrius Bucinskas − *Department of Polymer Chemistry and Technology, Kaunas University of Technology, Kaunas LT-51423, Lithuania*

Complete contact information is available at: https://pubs.acs.org/10.1021/acssuschemeng.3c04011

Author Contributions

D.V., B.F.M., and J.V.G. designed the research. D.G. and J.S. performed synthesis. L.V. and D.V. were responsible for the photophysical studies. M.M. was responsible for thermal analyses. A.A.P. and B.F.M. performed DFT calculations. A.B. was responsible for single-crystal X-ray analysis. D.V., B.F.M., and J.V.G. wrote the manuscript with support and contributions from all authors.

Notes

The authors declare no competing financial interest.

■ ACKNOWLEDGMENTS

This project has received funding from the Research Council of Lithuania (Project "ELOS" S-MIP-21-7), the Ministry of Science and Education of Ukraine (Project 0122U000760), and the Wenner-Gren Foundation (Project GFU2022-0036).

■ REFERENCES

(1) Tan, H.; Dang, R. Review of Lighting Deterioration, Lighting Quality, and Lighting Energy Saving for Paintings in Museums. *Build. Environ.* **2022**, *208*, No. 108608.

(2) Islam, N. U.; Usman, M.; Rasheed, S.; Jamil, T. White Light-Emitting Diodes: Past, Present, and Future. *ECS J. Solid State Sci. Technol.* **2021**, *10*, 106004.

(3) Phelan, G. M. OLED Lighting Hits the Market. *Inf. Dispersion* **2018**, *34* (1), 10−15.

(4) Ying, S.; Liu, W.; Peng, L.; Xiao, S.; Yang, D.; Qiao, X.; Chen, J.; Wang, L.; Ma, D. Efficient Exciton Regulation for High-Performance Hybrid White Organic Light-Emitting Diodes with Superior Efficiency/CRI/Color Stability Based on Blue Aggregation-Induced Emission Fluorophor. *Org. Electron.* **2022**, *101*, No. 106425.

(5) Xiang, H.; Wang, R.; Chen, J.; Li, F.; Zeng, H. Research Progress of Full Electroluminescent White Light-Emitting Diodes Based on a Single Emissive Layer. *Light Sci. Appl.* **2021**, *10*, 206.

(6) Yang, Y.; Lowry, M.; Schowalter, C. M.; Fakayode, S. O.; Escobedo, J. O.; Xu, X.; Zhang, H.; Jensen, T. J.; Fronczek, F. R.; Warner, I. M.; Strongin, R. M. An Organic White Light-Emitting Fluorophore. *J. Am. Chem. Soc.* **2006**, *128* (43), 14081−14092.

(7) Karpiuk, J.; Karolak, E.; Nowacki, J. Tuneable White Fluorescence from Intramolecular Exciplexes. *Phys. Chem. Chem. Phys.* **2010**, *12*, 8804−8809.

(8) Wu, X.; Wang, L.; Hua, Y.; Wang, C.; Batsanov, A. S.; Bryce, M. R. A Carbazole−Oxadiazole Diad Molecule for Single-Emitting-Component White Organic Light-Emitting Devices (WOLEDs). *Tetrahedron* **2014**, *70* (11), 2015−2019.

(9) Chen, Z.; Ho, C. L.; Wang, L.; Wong, W. Y. Single-Molecular White-Light Emitters and Their Potential WOLED Applications. *Adv. Mater.* **2020**, *32*, 1903269.

(10) Mukherjee, S.; Thilagar, P. Organic White-Light Emitting Materials. *Dye. Pigment.* **2014**, *110*, 2−27.

(11) Kukhta, N. A.; Bryce, M. R. Dual Emission in Purely Organic Materials for Optoelectronic Applications. *Mater. Horizons.* **2021**, *8*, 33−55.

(12) Zhang, X.; Du, L.; Zhao, W.; Zhao, Z.; Xiong, Y.; He, X.; Gao, P. F.; Alam, P.; Wang, C.; Li, Z.; Leng, J.; Liu, J.; Zhou, C.; Lam, J. W. Y.; Phillips, D. L.; Zhang, G.; Tang, B. Z. Ultralong UV/Mechano-Excited Room Temperature Phosphorescence from Purely Organic Cluster Excitons. *Nat. Commun.* **2019**, *10*, 5161.

(13) Liu, H.; Pan, G.; Yang, Z.; Wen, Y.; Zhang, X.; Zhang, S. T.; Li, W.; Yang, B. Dual-Emission of Fluorescence and Room-Temperature Phosphorescence for Ratiometric and Colorimetric Oxygen Sensing and Detection Based on Dispersion of Pure Organic Thianthrene Dimer in Polymer Host. *Adv. Opt. Mater.* **2022**, *10* (12), 2102814.

(14) Shi, Y.; Wang, S.; Tao, W.; Guo, J.; Xie, S.; Ding, Y.; Xu, G.; Chen, C.; Sun, X.; Zhang, Z.; He, Z.; Wei, P.; Tang, B. Z. Multiple yet Switchable Hydrogen-Bonded Organic Frameworks with White-Light Emission. *Nat. Commun.* **2022**, *13* (1), 1882.

(15) Liu, X. W.; Zhao, W.; Wu, Y.; Meng, Z.; He, Z.; Qi, X.; Ren, Y.; Yu, Z. Q.; Tang, B. Z. Photo-Thermo-Induced Room-Temperature Phosphorescence through Solid-State Molecular Motion. *Nat. Commun.* **2022**, *13* (1), 3887.

(16) Wen, Y.; Liu, H.; Zhang, S. T.; Pan, G.; Yang, Z.; Lu, T.; Li, B.; Cao, J.; Yang, B. Modulating Room Temperature Phosphorescence by Oxidation of Thianthrene to Achieve Pure Organic Single-Molecule White-Light Emission. *CCS Chem.* **2021**, *3* (7), 1940−1948.

(17) Tomkeviciene, A.; Dabulienė, A.; Matulaitis, T.; Guzauskas, M.; Andruleviciene, V.; Grazulevicius, J. V.; Yamanaka, Y.; Yano, Y.; Ono, T. Bipolar Thianthrene Derivatives Exhibiting Room Temperature

Phosphorescence for Oxygen Sensing. *Dye. Pigment.* **2019**, *170*, No. 107605.
(18) He, Z.; Zhao, W.; Lam, J. W. Y.; Peng, Q.; Ma, H.; Liang, G.; Shuai, Z.; Tang, B. Z. White Light Emission from a Single Organic Molecule with Dual Phosphorescence at Room Temperature. *Nat. Commun.* **2017**, *8* (1), 416.
(19) Zhang, T.; Wu, Y.; Ma, X. Tunable Multicolor Room-Temperature Phosphorescence Including White-Light Emission from Amorphous Copolymers. *Chem. Eng. J.* **2021**, *412*, No. 128689.
(20) Khan, F.; Volyniuk, L.; Ghasemi, M.; Volyniuk, D.; Grazulevicius, J. V.; Misra, R. Efficient Monomolecular White Emission of Phenothiazine Boronic Ester Derivatives with Room Temperature Phosphorescence. *J. Mater. Chem. C* **2022**, *10*, 10347.
(21) Leitonas, K.; Tomkeviciene, A.; Baratte, G.; Dabuliene, A.; Punniyakoti, S. M.; Volyniuk, D.; Grazulevicius, J. V. Oxygen Sensing Properties of Thianthrene and Phenothiazine Derivatives Exhibiting Room Temperature Phosphorescence: Effect of Substitution of Phenothiazine Moieties. *Sensors Actuators B Chem.* **2021**, *345*, No. 130369.
(22) Pander, P.; Swist, A.; Turczyn, R.; Pouget, S.; Djurado, D.; Lazauskas, A.; Pashazadeh, R.; Grazulevicius, J. V.; Motyka, R.; Klimash, A.; Skabara, P. J.; Data, P.; Soloducho, J.; Dias, F. B. Observation of Dual Room Temperature Fluorescence-Phosphorescence in Air, in the Crystal Form of a Thianthrene Derivative. *J. Phys. Chem. C* **2018**, *122* (43), 24958−24966.
(23) Yang, Z.; Zhao, S.; Zhang, X.; Liu, M.; Liu, H.; Yang, B. Efficient Room-Temperature Phosphorescence from Discrete Molecules Based on Thianthrene Derivatives for Oxygen Sensing and Detection. *Front. Chem.* **2022**, *9*, No. 810304.
(24) Yamazaki, M. Industrialization and Application Development of Cyclo-Olefin Polymer. *J. Mol. Catal. A Chem.* **2004**, *213* (1), 81−87.
(25) Wang, S.; Yuan, J.; Xie, J.; Lu, Z.; Jiang, L.; Mu, Y.; Huo, Y.; Tsuchido, Y.; Zhu, K. Sulphur-Embedded Hydrocarbon Belts: Synthesis, Structure and Redox Chemistry of Cyclothianthrenes. *Angew. Chemie - Int. Ed.* **2021**, *60* (34), 18443−18447.
(26) Yuan, J.; Lv, W.; Li, A.; Zhu, K. A Self-Assembled M 2 L 2 Truncated Square and Its Application as a Container for Fullerenes. *Chem. Commun.* **2021**, *57*, 12848.
(27) Grimme, S. Do Special Noncovalent π-π Stacking Interactions Really Exist? *Angew. Chemie - Int. Ed.* **2008**, *47* (18), 3430−3434.
(28) Pander, P.; Swist, A.; Soloducho, J.; Dias, F. B. Room Temperature Phosphorescence Lifetime and Spectrum Tuning of Substituted Thianthrenes. *Dye. Pigment.* **2017**, *142*, 315−322.
(29) Liu, H.; Gao, Y.; Cao, J.; Li, T.; Wen, Y.; Ge, Y.; Zhang, L.; Pan, G.; Zhou, T.; Yang, B. Efficient Room-Temperature Phosphorescence Based on a Pure Organic Sulfur-Containing Heterocycle: Folding-Induced Spin-Orbit Coupling Enhancement. *Mater. Chem. Front* **2018**, *2*, 1853.
(30) Yuan, J.; Wang, S.; Ji, Y.; Chen, R.; Zhu, Q.; Wang, Y.; Zheng, C.; Tao, Y.; Fan, Q.; Huang, W. Invoking Ultralong Room Temperature Phosphorescence of Purely Organic Compounds through H-Aggregation Engineering. *Mater. Horizons* **2019**, *6*, 1259−1264.
(31) Qiu, W.; Cai, X.; Chen, Z.; Wei, X.; Li, M.; Gu, Q.; Peng, X.; Xie, W.; Jiao, Y.; Gan, Y.; Liu, W.; Su, S. J. A "Flexible" Purely Organic Molecule Exhibiting Strong Spin-Orbital Coupling: Toward Non-doped Room-Temperature Phosphorescence OLEDs. *J. Phys. Chem. Lett.* **2022**, *13* (22), 4971−4980.
(32) Janietz, S.; Wedel, A. Electrochemical Redox Behavior and Electroluminescence in the Mixed Energy-Sufficient System Thianthrene and 2-(4-Biphenyl)-5-(4-Tert-Butylphenyl)-1,3,4-Oxadiazole. *Adv. Mater.* **1997**, *9* (5), 403−407.
(33) Minaev, B. F.; Terpugova, A. F. Spin-Orbit Interaction in Charge-Transfer Complexes. *Soviet Phys. J.* **1969**, *10*, 1260−35.
(34) Hempe, M.; Kukhta, N. A.; Danos, A.; Batsanov, A. S.; Monkman, A. P.; Bryce, M. R. Intramolecular Hydrogen Bonding in Thermally Activated Delayed Fluorescence Emitters: Is There Evidence Beyond Reasonable Doubt? *J. Phys. Chem. Lett.* **2022**, *13* (35), 8221−8227.
(35) Keruckiene, R.; Volyniuk, D.; Leitonas, K.; Grazulevicius, J. V. Dual Emission Fluorescence/Room-Temperature Phosphorescence of Phenothiazine and Benzotrifluoride Derivatives and Its Application for Optical Sensing of Oxygen. *Sensors Actuators B Chem.* **2020**, *321*, No. 128533.
(36) Baryshnikov, G.; Minaev, B.; Ågren, H. Theory and Calculation of the Phosphorescence Phenomenon. *Chem. Rev.* **2017**, *117* (9), 6500−6537.
(37) Data, P.; Takeda, Y. Recent Advancements in and the Future of Organic Emitters: TADF- and RTP-Active Multifunctional Organic Materials. *Chem. - An Asian J.* **2019**, *14* (10), 1613−1636.
(38) Minaev, B. F. Quantum-Chemical Investigation of the Mechanisms of the Photosensitization, Luminescence, and Quenching of Singlet1Δg Oxygen in Solutions. *J. Appl. Spectrosc.* **1985**, *42*, 518−523.
(39) Minaev, B. F.; Lunell, S.; Kobzev, G. I. Collision-Induced Intensity of the $B^1\Sigma g^+ - a^1\Delta g$ Transition in Molecular Oxygen: Model Calculations for the Collision Complex O2 + H2. *Int. J. Quantum Chem.* **1994**, *50* (4), 279−292.
(40) Hirata, S.; Hirata, S. Recent Advances in Materials with Room-Temperature Phosphorescence: Photophysics for Triplet Exciton Stabilization. *Adv. Opt. Mater.* **2017**, *5* (17), 1700116.
(41) Bolton, O.; Lee, K.; Kim, H.-J.; Lin, K. Y.; Kim, J. Activating Efficient Phosphorescence from Purely Organic Materials by Crystal Design. *Nat. Chem.* **2011**, *3*, 205−210.
(42) Wang, S.; Cheng, Z.; Han, X.; Shu, H.; Wu, X.; Tong, H.; Wang, L. Efficient and Tunable Purely Organic Room Temperature Phosphorescence Films from Selenium-Containing Emitters Achieved by Structural Isomerism. *J. Mater. Chem. C* **2022**, *10*, 5141.
(43) Yue, L.; Sun, Q.; Zhang, Y.; Wang, Y.; Cui, S.; Zhang, H.; Xue, S.; Yang, W. Organic Phosphor Doped Thermoplastics with Ultralong and Memorable Room Temperature Phosphorescence Different from Crystals. *Chem. Eng. J.* **2022**, *433*, No. 134307.

https://doi.org/10.1021/acssuschemeng.3c04011
ACS Sustainable Chem. Eng. 2023, 11, 16914−16925